2021 43rd Annual International Conference of the
IEEE Engineering in Medicine & Biology Society (EMBC)
Oct 31 - Nov 4, 2021. Virtual Conference

# Impact of Local Electrodes on Brain Stroke Type Differentiation using Electrical Impedance Tomography*

Hannah Lee, Jared Culpepper, *Graduate Student Member, IEEE*, Ali Farshkaran, Barry McDermott, and Emily Porter, *Member, IEEE*

***Abstract*— Electrical impedance tomography (EIT) of the head has the potential to provide rapid characterization of brain stroke. This study builds on previous work by implementing a more anatomically complex head model, contrasting results of bleed and clot simulations, and by establishing the electrodes which dominate in voltage difference measurements. This work provides the basis for machine learning with clusters of small numbers of electrodes as unique features for stroke-type detection and differentiation.**

***Clinical Relevance*— This application of EIT can aid in early detection, classification, and localization of brain stroke, allowing for faster treatment.**

## I. Introduction

Stroke is one of the most common causes of death worldwide [1]. Almost 800,000 Americans have a stroke each year [2], and as a result stroke is a leading cause of morbidity and serious long-term disability [2].

Early identification of a stroke is pivotal to successful treatment. The treatment approach depends on the cause of the stroke (as a bleed or clot), and therefore it is important to differentiate the root cause as quickly as possible. Current approaches typically include magnetic resonance imaging (MRI) or computed tomography (CT) scans upon arrival at the hospital. However, electrical impedance tomography (EIT) has been proposed as a complementary modality [3] that could enable differentiation of stroke type in the ambulance, leading to faster triage at the hospital and faster delivery of therapies. Earlier delivery of treatment leads to increased survival rates and decreased morbidity rates [2].

EIT is a low-cost, non-invasive imaging modality [4], that has potential to discriminate between stroke types based on the changes in impedances (or conductivities) of tissues in the head resulting from each type of stroke [3]. To date, EIT for stroke detection and differentiation has shown great promise with work in [3], [5], and [6] specifically using machine learning-based approaches to classify stroke type. Many variables have already been considered, but there are still a number of other factors which can impact the practical reliability of this technology. Additionally, further work in developing a more anatomically accurate model strengthens the credibility of the proposed use of EIT. Therefore, presented in this work is a study of which electrodes in an EIT stroke detection system dominate in voltage difference measurements depending on the location and type of stroke. Additionally, the highly conductive layer of cerebrospinal fluid (CSF) between the meninges and the brain is included in this simulation model to analyze its impact on the EIT measurement data. Finally, multiple lesion locations, sizes, and conductivities representing both bleed and clot cases are modeled, with the most informative results presented in this article.

## II. Methodology

In this section, the model of the head and lesions are described. Then, the simulation set-up is detailed. Lastly, the applied analysis of the resulting data is overviewed.

### A. Modeling of the Head and Lesions

The baseline model used in this study is a simplified but anatomically accurate three-layer head model consisting of an outer layer of skull and skin aggregate, a middle layer of CSF, and an inner volume of brain tissue aggregate. This baseline model is also compared with a simple two-layer model that does not contain the layer of CSF, in order to compare the results. The head and brain models were initially derived from MRI images [7] and were obtained for this study from the open source data available at [3] (in the form of stereolithography (STL) files). The model volumes are reduced by 41% from their realistic dimensions [3] to improve computation times and our later ability to fabricate the model. The model volumes are provided in Table I.

In the three-layer model, the CSF layer is subtracted from the skull layer, with the brain volume remaining the same in both cases with and without CSF. The CSF layer is approximately 5 mm in thickness (3 mm in the model), consistent with the average thickness of CSF [8], though CSF thickness varies widely throughout the cranial cavity. We note that the conductivity of CSF has been reported across a range of values, e.g., 1-2.5 S/m [9]. Here we choose the lower limit as the best-case (lowest loss) scenario. This decision was made to show the importance of CSF modeling, as it is expected that even in the best case scenario, the added CSF layer will have a significant impact on the voltage data.

TABLE I. Characteristics of each tissue type included in the head models.

| Tissue Type | Conductivity (S/m) | Model Volume (mL) | Realistic Volume (mL) |
|---|---|---|---|
| Skull/skin aggregate | 0.1 | 1972 | 3343 |
| CSF | 1.0 | 122 | 206.5 |
| Brain aggregate | 0.3 | 773 | 1310 |
| Bleed | 0.7 | 5.9-17.7 | 10-30 |
| Ischemic | 0.1 | 5.9-17.7 | 10-30 |

*Research supported by UT Austin Department of Electrical and Computer Engineering Start-up Funds, and the Dr. Brooks Carlton Fowler Endowed Presidential Graduate Fellowship in Electrical and Computer Engineering.

H. Lee, J. Culpepper, A. Farshkaran, and E. Porter are with the University of Texas at Austin, 2501 Speedway, Austin, TX 78712, United States (corresponding author phone: 512-232-8114; e-mail: Emily.porter@austin.utexas.edu).

B. McDermott is with the National University of Ireland Galway, Galway, Ireland, H91 TK33 (e-mail: barryjames.mcdermott@nuigalway.ie).

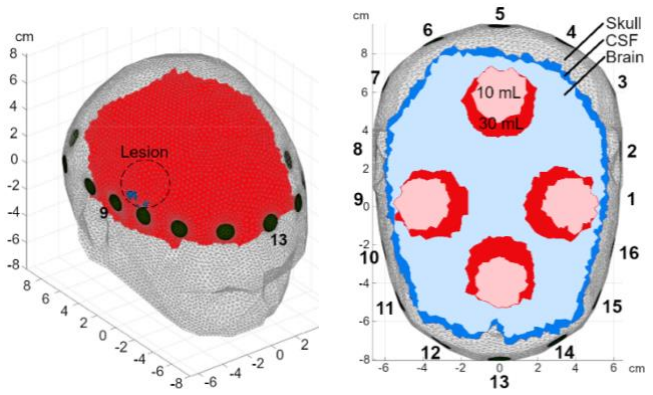


Figure 1. Example image of a head model with a lesion in the right hemisphere of the brain, and a diagram of model layers including the 8 lesion locations, 2 lesion volumes, and the 16 electrodes labeled.

In total, six different head models were generated, each with different relative sizes of the layers of the head model. With each of these head models, eight lesion variations were compared to the normal case. However, results from only one of these variations is presented as the variations all resulted in the same trends in terms of lesion detection.

To simulate a lesion produced by stroke in the brain, a sphere is placed in the brain volume of each model, and its conductivity is changed to represent a bleed (hemorrhagic stroke) or ischemic tissue (ischemic stroke, caused by a clot). Four lesion locations, at the front, back, right, and left sides of the head are studied, along with two lesion sizes in each location: 10 mL, and 30 mL. Simulated measurements of this model are compared to those of the non-lesion case, which is referred to as the 'normal' or 'healthy' case throughout this discussion.

The conductivities used for each tissue are provided in Table I. These values are based on those from [3], [9], and are representative of the properties at 50 kHz. Although other frequencies may also be of interest, 50 kHz is a common frequency point from past EIT studies and is conveniently available in commercial EIT measurement systems (e.g., the Swisstom Pioneer set) [3]. An example image of the head model with layers and lesion sizes and locations marked is shown in Fig. 1.

### B. *Simulation Set-up*

The STL files are meshed into a finite element model (FEM) using EIDORS [10] with Netgen [11] and Gmsh [12], and a ring of 16 electrodes is meshed around the outer layer of the model with the mesh appropriately refined where the electrodes make contact [13]. EIDORS simulates the injection of current based on the head models and forward solves to find the expected voltage measurements across pairs of electrodes. In each measurement, there are four electrodes involved: the two electrodes serving as the current injection pair and two electrodes for each voltage measurement. This measurement is repeated with all other electrode pairs serving as the current injection pair using a skip-two configuration [14]. The resulting voltage data can then be used to infer the conductivity distribution of the region, or changes in the conductivity distribution of the region.

For each unique head model, the voltage measurements are simulated over 250 trials with a pre-configured signal-to-noise ratio (SNR) that determines the amount of random noise that is added in the simulated measurements. SNRs from 20 to 120 dB are investigated and presented in Section III.A.

### C. *Description of Analysis of Dominant Contributors*

The difference between the lesion cases and the healthy non-lesion cases is calculated to demonstrate the deviation from the baseline voltage measurements when a lesion is present in the brain. The mean and the standard deviation of this difference across 250 repeated simulations are calculated for each measurement/injection electrode pair (defined as one measurement 'channel') for both the bleed case and clot case and across the different head models and lesion sizes. The mean of the differences is plotted in Fig. 2 for an example case of a 30 mL lesion on the right side of the head (results for both bleed and clot are provided), where the area within one standard deviation from the mean is shaded. The electrode position combinations are the measurements in sequential order. For example, in Fig. 2 and Fig. 3, position '1' corresponds to current injection pair 1-4, measurement pair 5-2; position '2' corresponds to 1-4, 6-3; and so forth. While each voltage measurement is a discrete point, they are interpolated and plotted as a continuous line to improve the readability of the plots.

For the purposes of this work, the dominant contributors are defined as the measurement and injection electrode pairs (i.e., the channels) that are the most essential for lesion detection and differentiation. The dominant contributing

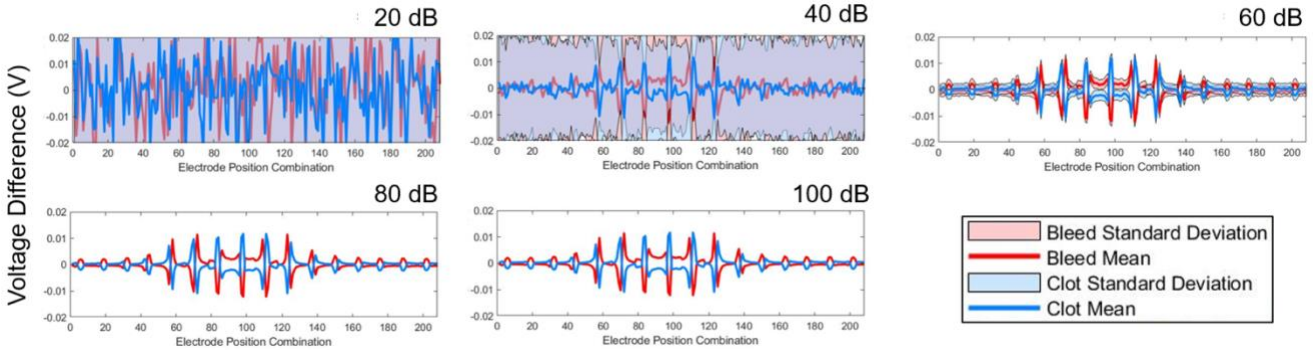


Figure 2. Mean (solid trace) and standard deviation (shaded region) of voltage differences between lesion and normal head models: for bleed (red traces) and for clot (blue traces). The voltage differences are shown for five noise levels: 20 dB, 40 dB, 60 dB, 80 dB, and 100 dB. (The 120 dB case is not shown, as it appears visually identical to the 100 dB case.) The plots are for the scenario of a 30 mL lesion, on the right side of the head.

electrodes are extracted from the simulated voltage measurements. For each unique head model, the absolute difference between the voltage measurements of the lesion case and normal case is calculated. Of these absolute differences, the five electrode position combinations that observed the greatest difference in voltage measurement from the normal case are noted for each repetition of the simulation.

The schematic of the head model in Fig. 1 shows the position of all 16 electrodes and their orientation, in addition to the approximate location and size of the lesion. In the head plots shown in Fig. 4 and Fig. 5, the current injecting electrodes are connected by a solid line, while the voltage measuring electrodes are indicated by a dashed line from the midpoint of the associated solid line to each measuring electrode. Each time an electrode combination is repeated in another simulation's dominant contributors, the thickness of the lines is increased. Therefore, thicker lines represent the electrode position combinations that more frequently occur in the top 5 most dominant contributors.

## III. Results

In this section, the voltage difference data and the dominant contributing electrodes are analyzed. Then, the effect of including CSF in the head models is investigated.

### A. Voltage Data

In this section, all results reported are those from head models that include the CSF layer. As expected, the magnitude of the simulated voltage difference between the normal and the bleed or clot case is the greatest in electrode combinations that are nearest to the lesion. This pattern is consistent for all head models and lesion locations. However, the head model and the location of the lesion have a minimal effect on the shape and the magnitude of the voltage differences. Similarly, the size of the lesion negligibly affects the shape of the voltage difference plot, but smaller lesions result in a smaller voltage difference than larger lesions as expected.

SNR contributes to the variability in the voltage differences. As SNR increases, the shaded area between one standard deviation above and below the mean decreases. At an SNR of 20 dB, the voltage difference is nearly undetectable due to the high variability of the measured signal. At 40 dB, the difference pattern is more noticeable, though reliability may be limited in more complex scenarios. However, at SNRs of 60 dB and above, a strong pattern is detectable which tends to correlate directly with the conductivity of the added lesion. To better gauge the efficacy of measuring lower SNRs, the raw voltage data may be analyzed by machine learning (ML) in future work to identify subtle patterns.

For the same lesion size and location in a particular head model, the electrode combinations that result in a positive difference for the bleed case generate a negative difference in the clot case and vice versa, creating voltage difference plots that approximately mirror each other. As bleeds are more conductive than brain while ischemic tissue is less conductive than brain, these results align with expectations.

### B. Dominant Contributors

In the test cases, the electrodes nearest the lesion consistently detect the greatest deviation in voltage from the healthy case, and it is these channels which are classified as the dominant contributors for each trial. The dominant contributors tend to occur where measurement electrodes intersect the path between the current injection electrodes.

These patterns in the dominant contributors (given that the SNR is high enough to accurately detect the lesion) are consistent for both bleed and clot cases, with similar electrode combinations detecting the greatest change given the same

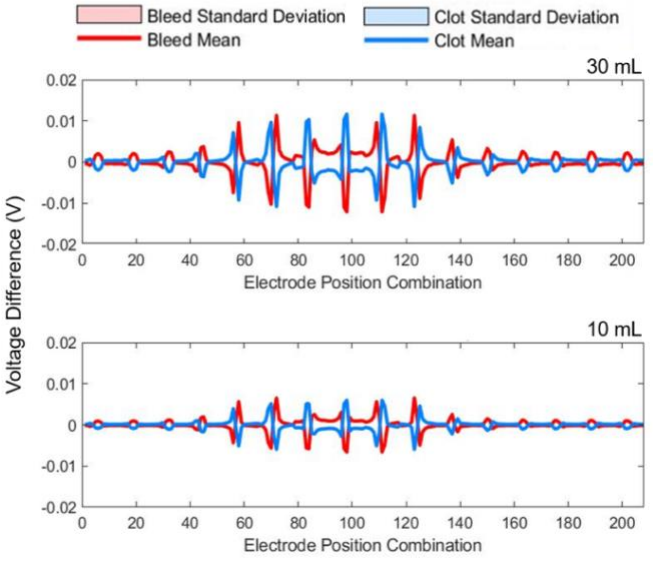


Figure 3. Mean and standard deviation (which is too low to be visible) of voltage differences between lesion and normal head models. The voltage differences are shown for two sizes of lesion: 30 mL and 10 mL, both on the right side of the head. The SNR is 120 dB for both graphs.

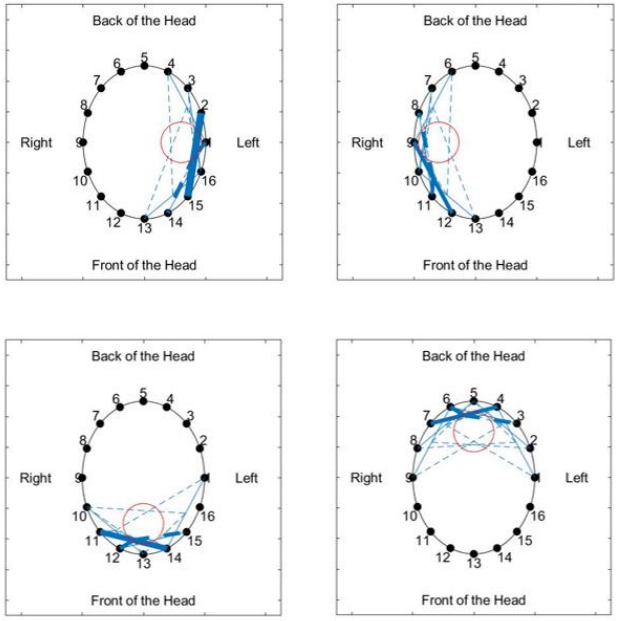


Figure 4. Plot of dominant contributors, for 30 mL size bleeds at four different locations in the head (for SNR of 120 dB).

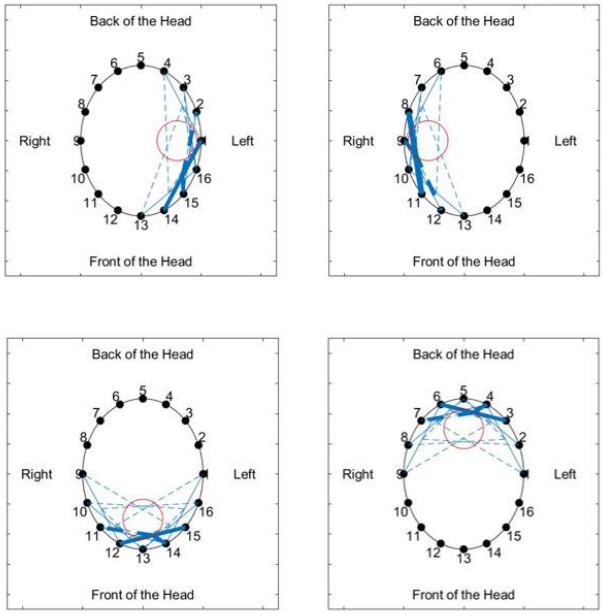


Figure 5. Plot of dominant contributors, for 30 mL size clots at four different locations in the head (for SNR of 120 dB).

head model, lesion location, and lesion size. Similarly, the size of the lesion and the head model used do not play a major role in the resulting dominant electrodes.

### C. CSF vs. no CSF

Generally, the inclusion of the CSF layer minimally changes the shape of the voltage difference plot, as shown in Fig 6, and similarly for the dominant contributing electrodes. However, including the CSF scaled down the magnitude of the majority of the voltage difference by approximately 25%.

Similar trends are found for both lesion types and across the lesion sizes and positions. Though the inclusion of CSF does not greatly change the shape of the signal, the attenuation of the signal is significant enough that it is important to consider the CSF layer in the model to make the loss more realistic, as it will impact feasible detectability. However, the model assumes the CSF layer to be of approximately constant thickness outside the perimeter, which is not realistic. Despite this limitation, since the same CSF layer is used in both healthy and non-healthy cases, it is expected that correcting this limitation will have a minimal effect on the data.

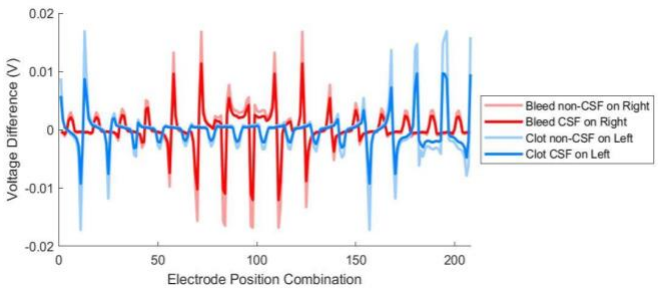


Figure 6. Plot of mean voltage difference with and without CSF: for a bleed (red trace, for bleed located on right side of head); and a clot (blue traces, for clot located on left side of head). Both lesions are 30 mL in size, simulated with an SNR of 120 dB.

## IV. Discussion and Conclusions

In this work, we have shown that the channels with electrodes nearest the lesion consistently detect the greatest difference from the normal case across various head models, lesion sizes, lesion locations, and SNRs. If only few electrodes contribute prominently to the detection of the lesion, then future work could investigate using groups of small arrays instead of a 16-element electrode array, thereby decreasing the amount of required circuitry, memory storage, and cost. Additionally, a hemorrhagic stroke and an ischemic stroke result in opposite differences from the normal case, thereby demonstrating that EIT has promising results in the differentiation of stroke types, given an SNR of 60 dB or higher for accurate detection. Future work includes machine learning classification, improvements in the accuracy of the head models, considering intra- and inter-individual variability in parameters, and further differentiation of stroke types and locations.

## References


[1] W. Johnson, O. Onuma, M. Owolabi and S. Sachdev, "Stroke: a global response is needed," Bulletin of the World Health Organization, vol. 94, no. 9, pp. 633-708, 2016.

[2] Centers for Disease Control and Prevention, “Stroke Facts,” Available online: https://www.cdc.gov/stroke/facts.htm, [Accessed 04-04-2021].

[3] B. McDermott, M. O’Halloran, E. Porter, and A. Santorelli, “Brain Haemorrhage Detection using a SVM Classifier with Electrical Impedance Tomography Measurement,” *PLoS ONE*, vol. 13, no. 7, 2018.

[4] B. Brown, “Electrical impedance tomography (EIT): A review,” *Journal of Medical Engineering & Technology*, vol. 27, no. 3, pp. 97–108, Jan. 2003.

[5] J. P. Agnelli, A. Çöl, M. Lassas, R. Murthy, M. Santacesaria, and S. Siltanen, “Classification of stroke using neural networks in electrical impedance tomography,” *Inverse Problems*, vol. 36, no. 11, p. 115008, Nov. 2020.

[6] V. Candiani and M. Santacesaria, “Neural Networks for Classification of Strokes in Electrical Impedance Tomography on a 3D Head Model,” arXiv preprint arXiv:2011.02852, 2020.

[7] N. Dilmen. NIH 3D Print Exchange- Brain MRI. Available online: https://3dprint. nih.gov/discover/3DPX-002739 [Accessed 02-15-2017].

[8] F. B. Haeussinger, S. Heinzel, T. Hahn, M. Schecklmann, A.-C. Ehlis, and A. J. Fallgatter, “Simulation of Near-Infrared Light Absorption Considering Individual Head and Prefrontal Cortex Anatomy: Implications for Optical Neuroimaging,” *PLOS ONE*, vol. 6, no. 10, p. e26377, Oct. 2011.

[9] H. McCann, G. Pisano, L. Beltrachini, “Variation in Reported Human Head Tissue Electrical Conductivity Values,” *Brain Topogr.*, vol. 32, no. 5, pp. 825-858, 2019.

[10] Adler and Lionheart (2005), "Uses and abuses of EIDORS: An extensible software base for EIT," *Physiol. Meas.*, vol. 27, no. 5, pp. S25-42, 2006.

[11] Schoeberl J. Netgen [Internet]. Vienna, Austria: Vienna University of Technology; Available: https://ngsolve.org/

[12] C. Geuzaine and J.-F. Remacle, “Gmsh: A 3-D finite element mesh generator with built-in pre- and post-processing facilities,” *Int. J. Numer. Meth. Eng.*, vol. 79, no. 11, pp. 1309–1331, May 2009.

[13] B. Grychtol and A. Adler, “FEM Electrode Refinement for Electrical Impedance Tomography" *Ann. Intl. Conf. Engineering in Medicine and Biology Society (EMBC),* 2013.

[14] A. Adler and A. Boyle, “Electrical Impedance Tomography: Tissue Properties to Image Measures,” *IEEE Trans. Biomed. Eng.*, vol. 64, no. 11, pp. 2494-2504, 2017.